

INTRODUCTION

autoimmune condition referred to as thyroid eye disease (TED) [1 3]. It was reported that 25%-50% of patients ocular symptoms [4]. The typical clinical characteristics include eyelid retraction, ocular dyskinesia, diplopia, exophthalmos, and strabismus. Moreover, dysthyroid

optic neuropathy (DON) might develop into visual loss in severe cases [5 7]. TED is recognized as an inflammatory disease with orbital and extraocular muscle involvement. The primary pathogenesis is well known as immune-induced TSH receptor and IGF-1 receptor injury in ocular connective tissues (OCT) [8 10]. Although glucocorticoids [11], surgery [12], radiotherapy [13] and targeted drugs (tocilizumab [14] and teprotumumab [15]) can partially

benefit patients, promising therapies remain absent due to the side effects and high cost of current measures.

Most studies have proposed that the positive feedback effect of inflammatory cytokines runs throughout the TED process. Immune cells infiltrating periorbital tissues release inflammatory mediators to activate OFs, which in turn secrete cytokines to promote the homing and infiltration of immune cells [2, 5, 16]. However, current insights into the mechanisms of TED are still unclear. With the rise of high-throughput sequencing technology, potential biomarkers related to TED have emerged. Wescombe et al. [17] revealed that CASQ2 and SDH4 were highly expressed in TED via an autoimmunity trigger mechanism. Zhao et al. [18] found that differentially expressed genes (DEGs) associated with the cell cycle (UBE2C), encoding proteasome (PSMA1), and signal recognition particle (SRP14) could have significant involvement in the development of TED. Further investigation also identified several (e.g., PTX3, CCL2, HOXB2, SERPINA1, HSP90B1, and CANX) as novel biomarkers of TED [19–22]. Although these valuable studies enriched our understanding of the underlying pathological processes in different target tissues of TED, whether there is a regulatory relationship between DEGs in each target tissue remains unknown. Furthermore, the majority of investigations only emphasized DEG screening and pathway speculation without in-depth exploration and verification.

For the first time, we incorporated microarray information from the Gene Expression Omnibus (GEO) repository in our study and discovered the significant involvement of ferroptosis-associated genes in TED. We also employed machine learning to establish a ferroptosis-related diagnostic nomogram and validate its accuracy for TED. Moreover, we integrated the DEGs of the thyroid, lacrimal gland, and periorbital adipose tissue and used correlation analysis to investigate possible relationships. Furthermore, an analysis of immune infiltration was conducted to investigate possible relationships between DEGs and immune cells. All the findings will refresh our understanding of the development of TED and support novel directions for further exploration.

Data acquisition

We focused on two gene expression datasets (GSE105149 and GSE58331) related to TED, utilizing

(<https://www.ncbi.nlm.nih.gov/geo/>) [23–28]. Both microarray datasets originated from the same platform,

GPL570 [HG-U133_Plus_2] Affymetrix Human Genome U133 Plus 2.0 Array, with the organism *Homo sapiens* and an experimental type of expression profiling by array. According to the inclusion criteria for TED and normal lacrimal samples, 4 cases of TED and 7 control cases derived from GSE105149 [23] were included, as well as 8 cases of TED and 7 control cases derived from GSE58331 [24–28]. The raw expression matrix and annotation of the above samples were downloaded and integrated for subsequent bioinformatic analysis. We employed the ComBat function of the SVA package [29] in R (version 4.2.1) [30] to eliminate the batch effects and visualized the data distribution using different diagrams [31].

Screening of ferroptosis-related DEGs

To investigate whether ferroptosis is involved in the pathogenesis of TED, we first obtained the union set of genes associated with ferroptosis from both the *Homo sapiens* organism and the FerrDb V2 database (<http://www.zhounan.org/ferrdb/current/operations/download.html>) [32]. Then, ferroptosis-related DEGs (F-DEGs) were screened out via the intersection with the DEG set of TED.

Expression analysis and diagnostic value assessment

We assessed the differential expression of F-DEGs in 14 normal and 12 TED tissues, with data normalized and log2 transformed. To assess the diagnostic capability of F-DEGs in TED, we used receiver operating characteristic (ROC) curves to perform a series of analyses. To measure the diagnostic value, the area under the curve (AUC) was calculated. An AUC > 0 was defined as low accuracy [33].

Construction of the F-DEG-related diagnostic model

Based on the expression profiles above, we performed univariate binary logistic regression analysis using the glmnet package [34] in R to further screen variables. Then, the variables were included in the multivariate analysis and the model correlation test if they met the threshold of $p < 0.01$. F-DEGs were chosen for the diagnostic model, and their odds ratio (OR) was visualized by a forest diagram [35]. On this basis, we constructed an F-DEG-related diagnostic nomogram for TED patients. The model was calibrated [36] and evaluated by employing diagnostic ROC and decision curve analysis (DCA) to verify its precision and robustness. The concordance index (C-Index) and Akaike information criterion (AIC) [37, 38] were subsequently computed. Furthermore, we applied

LASSO regression [35, 39], which is a supervised machine learning method, to identify the most relevant variables for diagnostic model establishment. Calibration, diagnostic ROC, and DCA were performed

Gene enrichment analysis

We conducted Kyoto Encyclopedia of Genes and Genomes (KEGG) pathway analysis, as well as Gene

clusterProfiler

4.0.3, www.r-project.org) [30]. Bubble diagrams and circle plots were applied for visualization.

GSEA and GSVA

To further elucidate the mechanistic differences between the TED and normal groups, we included all the DEGs in gene set enrichment analysis (GSEA) [40]. GSEA offered three benefits over conventional enrichment: 1) genes were ranked according to their expression levels; 2) the object of analysis was a gene set rather than a single gene; and 3) the genes were compared to a predefined gene set. According to the annotation and description, we selected and downloaded reference data

Human Molecular Signatures Database (MSigDB) [41]. The results are displayed as biological process (BP), cell component (CC), molecular function (MF), and KEGG. For visualization, classic and ridge diagrams were employed, with the clusterProfiler package [42] in R used to calculate the normalized enrichment score (NES) and false discovery rate (FDR).

Gene set variation analysis (GSVA), a non-parametric unsupervised algorithm, transforms a gene-sample expression matrix into a specific gene set-sample expression matrix [43]. Using this strategy, we sorted the genes based on their cumulative density distribution and computed the rank statistics for further downstream analysis. The MSigDB

in GSVA, and the route of enrichment differences between the test and control groups were compared as a result.

WGCNA

Weighted gene correlation network analysis (WGCNA) is defined as a systematic biological technique for characterizing gene relationship patterns across samples. By examining the interrelation between the gene set and its associations with other phenotypes,

it may be used to identify gene sets with significant covariation as well as possible biomarker genes or therapeutic targets [44]. We used this method to build a gene co-expression network and discovered essential modules consisting of the interconnected gene sets in both TED and normal samples.

Protein-protein interaction (PPI) network and hub gene identification

We extracted the most relevant gene modules from WGCNA and used them to interact with DEGs. The DEG

<http://string-db.org/>) [45], which allows functional proteomic interaction analysis. The main parameters were set

and Experiments and

default. Next, we built the TED-related PPI network using Cytoscape (version 3.9.1) [46, 47], a free program for network data integration and visualization. We investigated the TED-related hub genes further in Cytoscape using the MCC algorithm of the CytoHubba module [48]. The top ten hub gene networks were categorized, as were the top five hub gene networks discovered by the MCODE module [49].

We used ridge diagrams to show the distribution of the aforesaid hub genes (H-DEGs) in TED and normal tissues according to their expression levels. Moreover, the diagnostic capability of these genes was evaluated by employing ROC and AUC.

Correlation analysis of immune cell infiltration

While the importance of the immune response in TED has been acknowledged, limited research has delved into the involvement of immune cells and inflammatory factors in the disease and their specific pathways. It is crucial to conduct immune infiltration studies at TED to uncover novel mechanisms and potential therapeutic targets related to immunity. To estimate the abundance of different cell types within a mixed population based on gene expression profiles, we utilized CIBERSORTx, an analytical tool (<https://cibersortx.stanford.edu/>) [50]. This program was employed to calculate the levels of 22 immune cell types in both the TED and normal groups. The distribution and infiltration abundance of these 22 immune cells between the test and control groups were visually represented using box plots and histograms. Additionally, we examined how F-DEGs and H-DEGs relate to immunocytes as well as their interaction with both TED and normal tissues.

S	T	Z	Z	Y
Gene	F:5'-3'			R:5'-3'

further inquiries can be directed to the corresponding author(s).

All data and original files in our work are freely available under a Creative Commons Attribution 4.0 International license.

All methods were carried out in accordance with relevant guidelines and regulations.

Figure 1 demonstrates the whole design and procedure of this study.

Data normalization

To comprehensively evaluate and analyse variations in gene expression, we combined and merged two distinct datasets. We implemented a standardized process to remove batch effects and normalize the original data, enhancing the accuracy and efficiency of subsequent

data analysis. The processed data exhibited significantly superior standardized signal intensity compared to the initial data processing stage (Figure 2A, 2B). Using principal component analysis (PCA), the standardized data exhibited improved within-group repeatability and between-group discriminability (Figure 2C, 2D). The uniform manifold approximation and projection (UMAP), a technique for reducing dimensions, showed consistent results regarding the data distribution as above (Figure 2E, 2F).

F-DEG screening

A total of 12 TED samples and 14 control samples comprised the consolidated data. After examining the variations in gene expression among the two groups, 414 DEGs were screened by applying the filter criterion $|\text{Log}_2\text{FC}| > 1$ and $p < 0.05$. The results are depicted using a heatmap (Figure 2G), which displays the panorama and clusters of DEGs, with 73 upregulated

genes and 341 downregulated genes further visualized as a volcano diagram (Figure 2H).

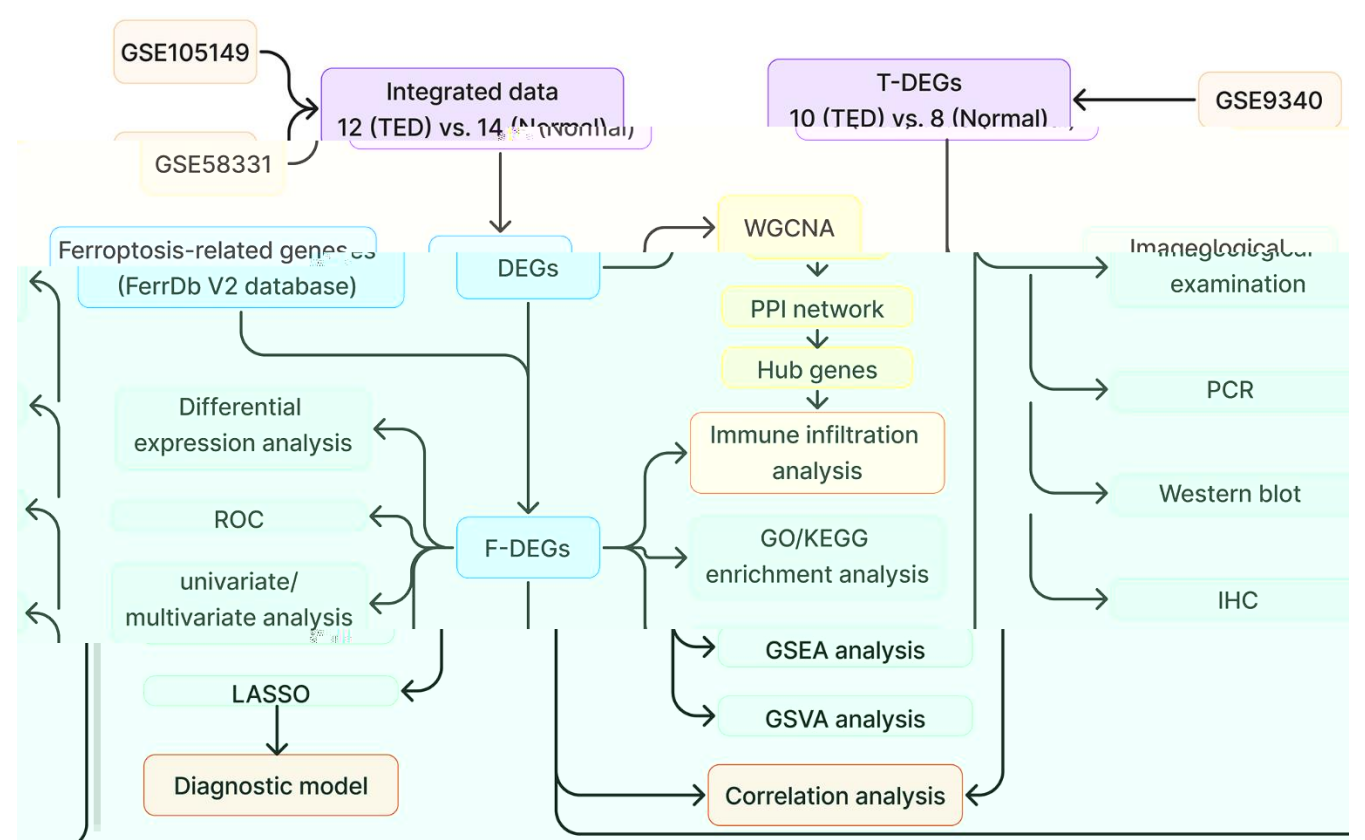
Through the integration of ferroptosis driver, ferroptosis suppressor, and ferroptosis marker gene sets, 322 ferroptosis-related genes were obtained (Figure 2I). By further intersecting with the DEGs above, we identified 11 ferroptosis-related DEGs (F-DEGs) (Figure 2J). The expression patterns of these 11 F-DEGs were detailed and are shown in a violin plot (CP, CDH1, TFAP2A, MDM4, TF, DNAJB6, OSBPL9, IDH1, MYCN, PEX3, and EMC2) (Figure 3A). MYCN stood out as a gene that was specifically overexpressed in the TED group ($p < 0.001$), while the majority of genes showed increased expression in the normal group (all $p < 0.05$) (Figure 3A).

Clinical value assessment of F-DEGs

Additionally, we conducted an evaluation to ascertain the diagnostic value of the F-DEGs for TED. The findings showed that every single F-DEG exhibited exceptional diagnostic performance for TED (TF: AUC = 0.774, DNAJB6: AUC = 0.911, OSBPL9: AUC =

0.881, IDH1: AUC = 0.845, CP: AUC = 0.821, CDH1: AUC = 0.821, TFAP2A: AUC = 0.792, MDM4: AUC = 0.827, MYCN: AUC = 0.899, PEX3: AUC = 0.935, and EMC2: AUC = 0.845) (Figure 3B).

We further performed a univariate logistic analysis of F-DEGs to examine their associations with TED diagnosis. In the diagnosis of individuals with TED, MYCN was identified as a significantly important independent factor (OR = 14.831, 95% confidence interval (CI) = 12.938-16.723, $p = 0.005$). The examination of other F-DEGs, on the other hand, revealed a possibly unfavorable effect on the diagnosis of TED (all OR < 1, $p < 0.05$) (Figure 3C). Genes that had a statistical significance of $p < 0.01$ were chosen for inclusion in the multivariate Cox regression analysis. EMC2 potentially had a favorable association with TED (OR = 4.459, 95% CI = 0.446-8.472). PEX3 (OR = 0.003, 95% CI = -6.285-6.292), DNAJB6 (OR = 0.616, 95% CI = -5.291-6.523), OSBPL9 (OR = 0.064, 95% CI = -7.218-7.347), and MYCN (OR = 0.066, 95% CI = -8.304-8.435), on the other hand, revealed an inverse correlation (Figure 3D). However, no statistical significance supported these correlations (all $p > 0.05$).



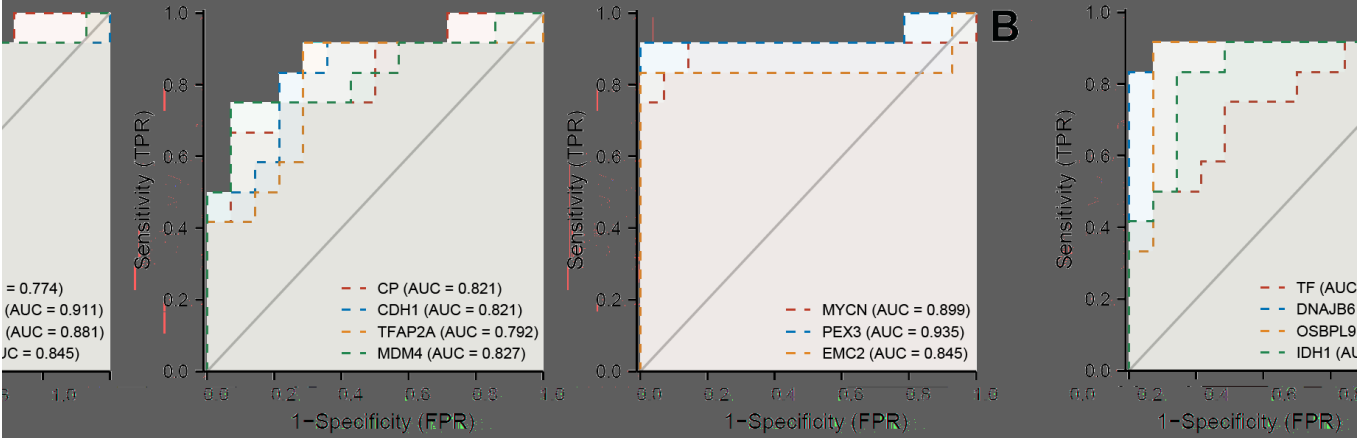
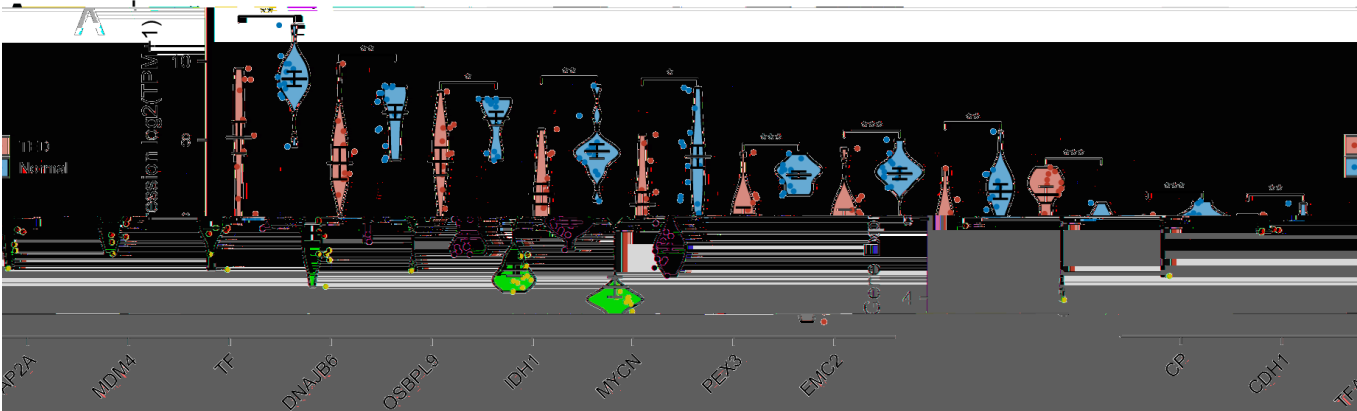
Establishment and validation of the diagnostic prediction model

Based on the above results, we first integrated the five most statistically relevant genes and constructed a

ferroptosis-related nomogram for TED risk prediction (Figure 4A). PEX3 made the greatest contribution and was recognized as an important independent diagnostic factor in addition to the other four factors. This model demonstrated good accuracy and robustness in



z z s z z s t s s

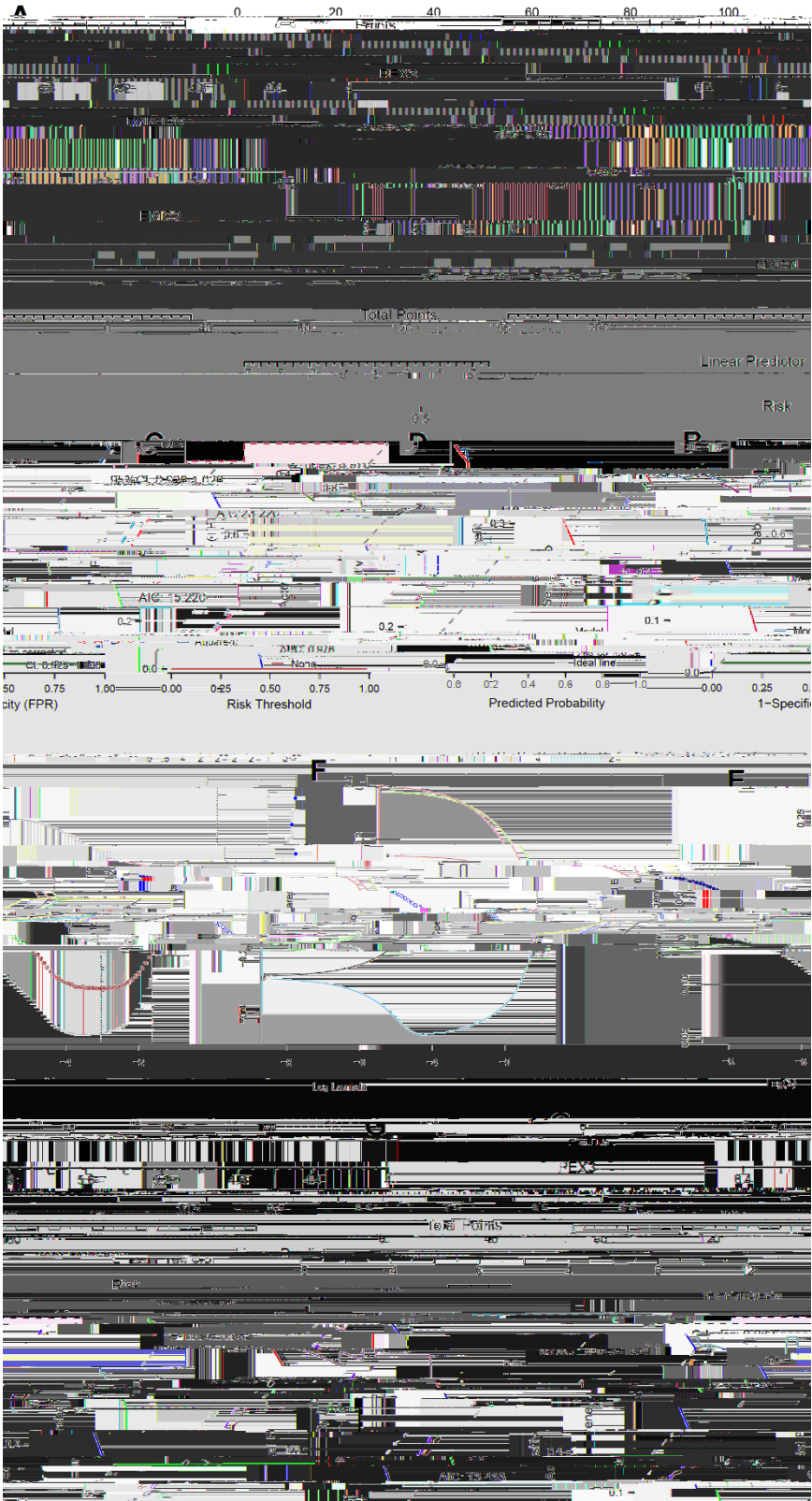


Gene	Sample(N)	OR(95% CI) Univariate analysis	P value Univariate analysis
MYCN	n=26(case=12)	14.831 (12.938 - 16.723)	0.005
PEX3	n=26(case=12)	0.012 (-3.091 - 3.114)	0.005
EMC2	n=26(case=12)	0.134 (-1.334 - 1.602)	0.007
TF	n=26(case=12)	0.325 (-0.636 - 1.285)	0.022
DNAJB6	n=26(case=12)	0.025 (-2.724 - 2.792)	0.006
OSBPL9	n=26(case=12)	0.074 (-1.774 - 1.922)	0.006
IDH1	n=26(case=12)	0.137 (-1.388 - 1.663)	0.011
CP	n=26(case=12)	0.211 (-1.101 - 1.524)	0.02
CDH1	n=26(case=12)	0.233 (-0.955 - 1.421)	0.016
TFAP2A	n=26(case=12)	0.220 (-1.065 - 1.505)	0.021
MDM4	n=26(case=12)	0.152 (-1.339 - 1.644)	0.013

Gene	Sample(N)	OR(95% CI) Multivariate analysis	P value Multivariate analysis
PEX3	n=26(case=12)	0.002 (-6.295 - 6.292)	0.071
DNAJB6	n=26(case=12)	0.018 (-5.291 - 5.293)	0.072
OSBPL9	n=26(case=12)	0.084 (-1.218 - 1.347)	0.46
EMC2	n=26(case=12)	4.459 (0.446 - 4.472)	0.465
MYCN	n=26(case=12)	0.008 (-0.304 - 0.435)	0.524

T z f i f i s z

P P P



Z SZ T

ZZ S

T S

P

P

P

providing diagnostic prediction clinical episodes (C-index = 0.976, 95% CI = 0.926-1.026, AIC = 23.220) (Figure 4B). We supplementally employed a time-dependent ROC curve to evaluate the diagnostic precision of this model (AUC = 0.976, 95% CI = 0.925-1.000) (Figure 4C) and performed DCA to assess the practicality of this model (AIC = 15.220) (Figure 4D).

Furthermore, we adopted a machine learning strategy (LASSO regression) to filter the 11 F-DEGs for the most diagnostically valuable genes. The LASSO coefficients were calculated using a tenfold cross-verification procedure and presented as a variable trajectory diagram (Figure 4E, 4F). We subsequently established a new F-DEG-related diagnostic nomogram that included PEX3 and CP, both of which contributed equally to this prediction model (Figure 4G). This

□
-
index = 0.982, 95% CI = 0.943-1.021, AIC = 15.433)

were further confirmed by the time-dependent ROC curve (AUC = 0.982, 95% CI = 0.943-1.000) (Figure 4I) and DCA (AIC = 13.433) (Figure 4J).

Biological enrichment analysis

To delve deeper into the molecular mechanism of DEGs in TED, we employed GO and KEGG enrichment analyses. By setting a significance threshold of $p < 0.05$, we successfully identified the top 10 correlated pathways of BP and CC, the top 5 correlated pathways of MF, and the top 3 correlated pathways of KEGG.

to Golgi vesicle-

-coated

insertion into ER membrane by stop-transfer membrane-
 $p < 0.001$) were mainly involved in TED (Figure 5A). Consistently, CC pathways were also primarily associated with protein coating and membrane transport (all $p < 0.001$) (Figure 5B). Regarding MF, we noticed an enrichment

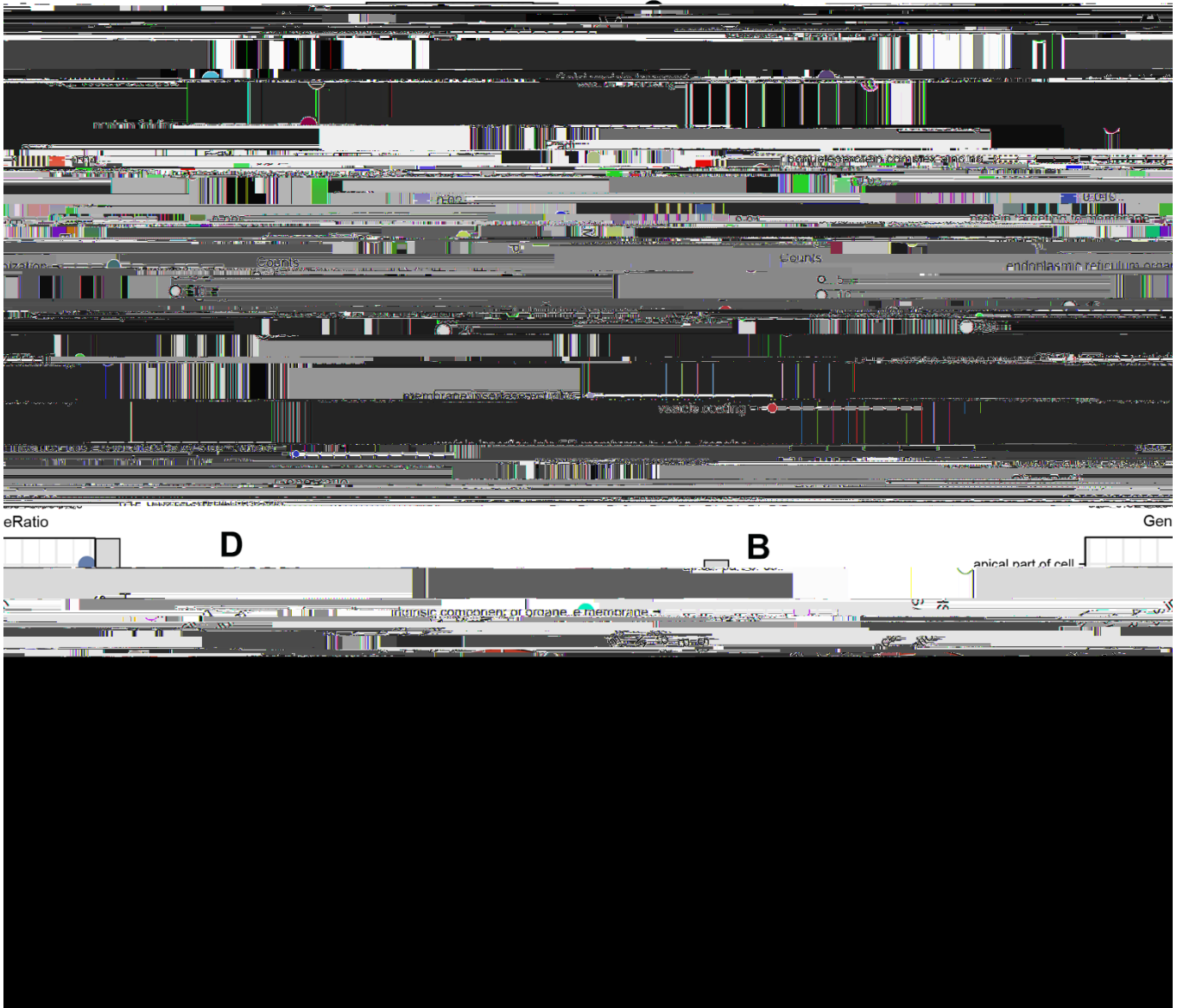
□

p

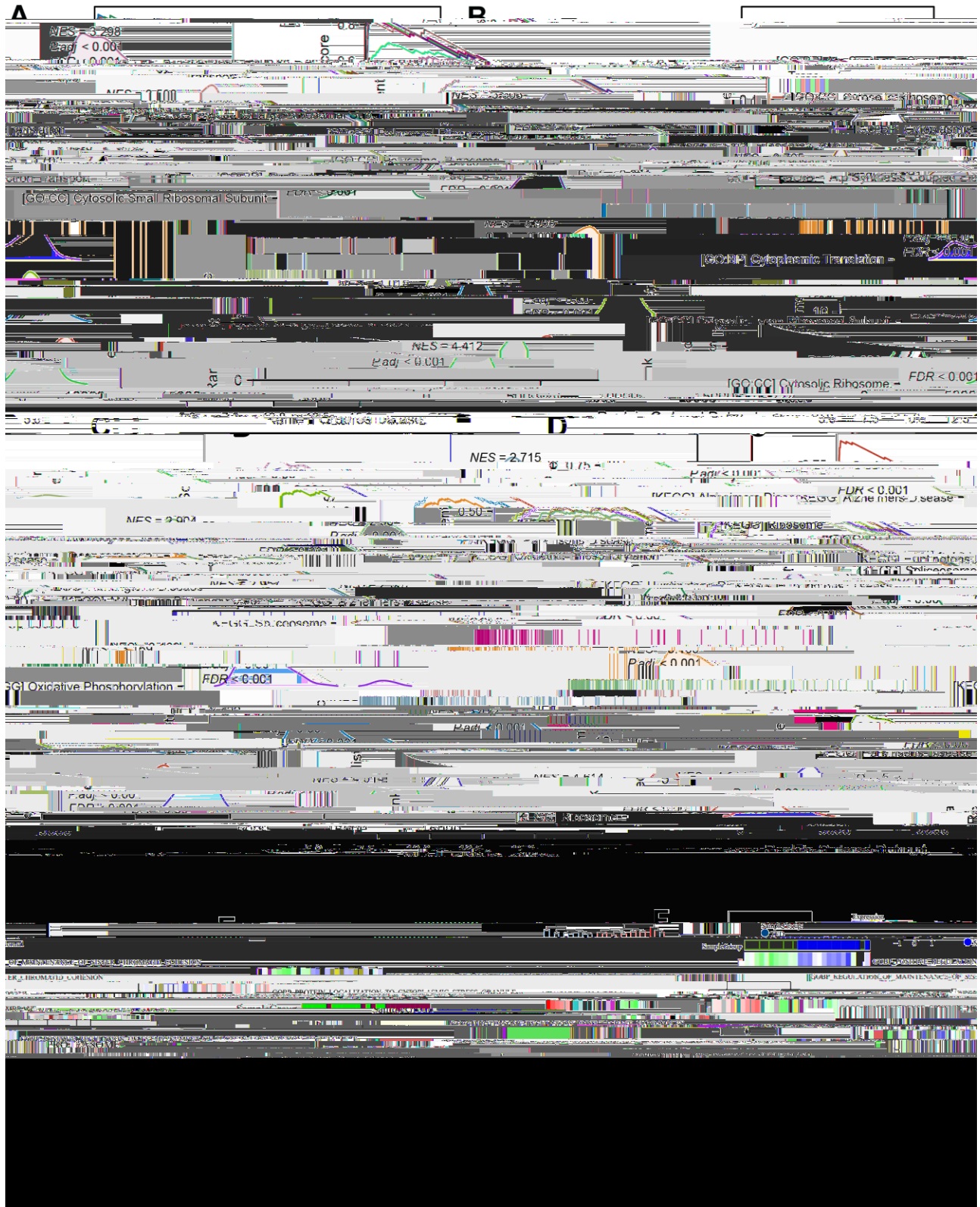
Next, we intersected the above two gene set modules with the DEGs and obtained 83 DEGs for the skyblue module and 188 DEGs for the blue module (Figure 8A). Based on the evidence from text mining, experiments, and databases, we constructed DEG-related PPI networks of 50 predicted functional partners (Figure 8B). Additionally, we selected the whole interaction network and the top 2 clusters from the DEGs to mine for potential hub genes. Using the MCC algorithm, the top 10 hub genes, including PSMA1, PSMA4, PSMA3, PSMA12, PSMA14, PSMA6, ITCH, SNRPG, SRSF1, and RBM25, were screened from the whole interaction network (Figure 8C). The top 5 hub genes of Cluster 1

(score = 7.000) were PSMA1, PSMA4, PSMA3, PSMA12, and ITCH (Figure 8D). Meanwhile, the top 5 hub genes of YKT6, COPB2, USO1, LMAN1, and RAB1A were included in Cluster 2 (score = 5.600) (Figure 8E).

A total of 15 hub gene-related DEGs (H-DEGs) were integrated. Ridge diagrams fully displayed the distribution differences of H-DEG expression in the TED ($p = 7.8\text{e-}61$) (Figure 8F) and normal groups ($p = 1.8\text{e-}18$) (Figure 8G). We further performed ROC curves to evaluate the diagnostic capacity of H-DEGs in TED. A remarkable accuracy of all H-DEGs in



T S Z Z
P P P

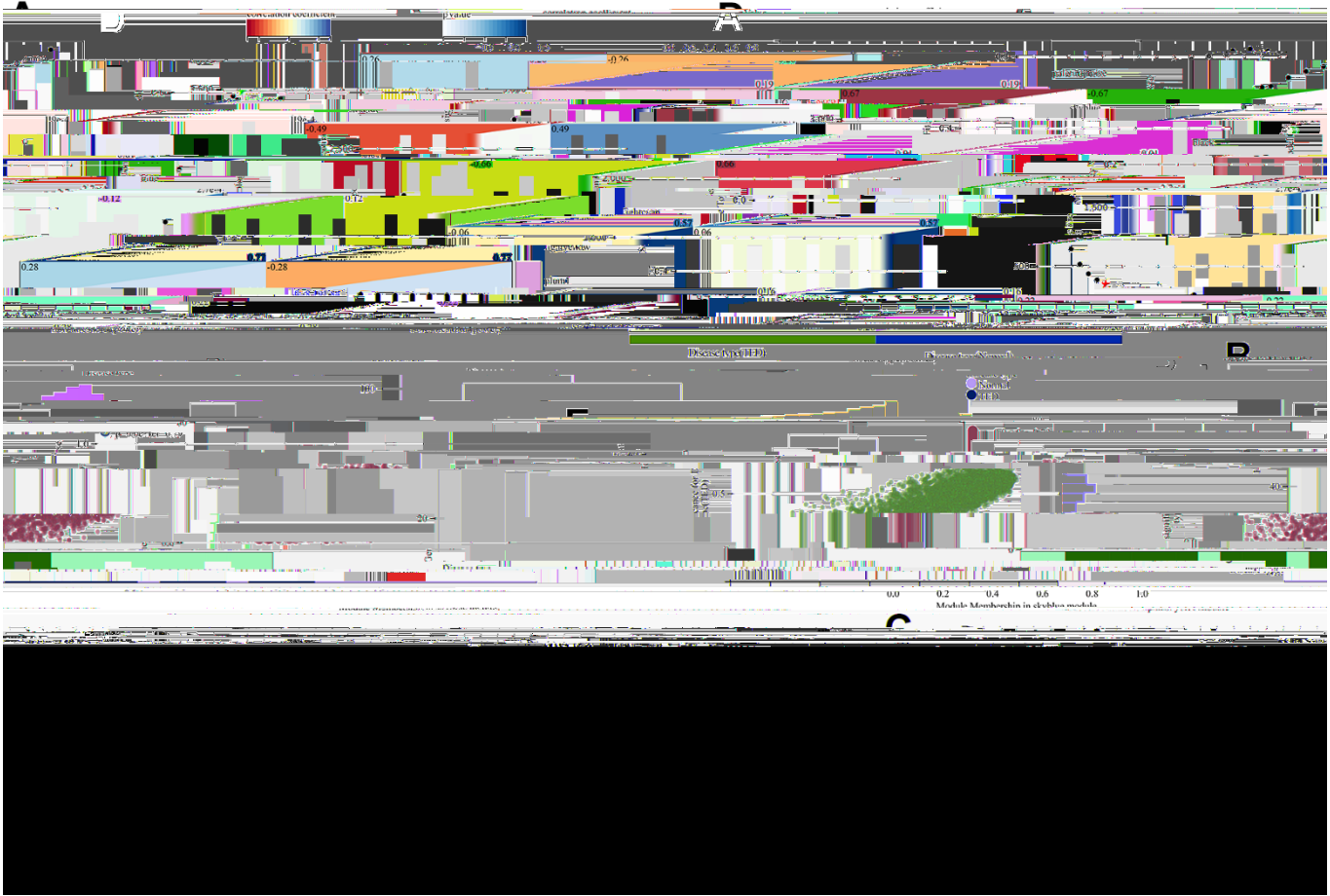


diagnosis was observed: SRSF1 (AUC = 0.917), SNRPG (AUC = 0.869), RBM25 (AUC = 0.887), PSMD6 (AUC = 0.929), PSMD14 (AUC = 0.905), COPB2 (AUC = 0.863), LMAN1 (AUC = 0.875), RAB1A (AUC = 0.851), YKT6 (AUC = 0.863), USO1 (AUC = 0.899), ITCH (AUC = 0.905), PSMA1 (AUC = 0.911), PSMA4 (AUC = 0.893), PSMA3 (AUC = 0.917), and PSMA12 (AUC = 0.905) (Figure 8H).

Immune infiltration analysis

We obtained 22 immune cell infiltration scores for lacrimal samples via the CIBERSORT algorithm. Regardless of whether TED or normal samples were taken, the component of plasma cells was the highest (Figure 9A). According to the infiltration abundance, the TED group had a higher degree of B-cell memory ($p < 0.01$), CD8 T cells ($p < 0.001$), and regulatory T cells (Tregs) ($p < 0.01$) infiltration than the normal group. In contrast, the infiltration levels of plasma cells ($p < 0.01$)

and resting memory CD4 T cells ($p < 0.05$) were higher in the normal group than in the TED group (Figure 9B). Furthermore, we examined the interactions of immune cells in lacrimal tissue, as well as their interactions with F-DEGs and H-DEGs. In the TED group, there was a strong positive correlation between M1 macrophages and naive B cells, resting mast cells and M2 macrophages, and activated mast cells and resting NK cells, while there was a strong negative correlation between resting memory CD4 T cells and plasma cells (all $p < 0.001$) (Figure 9C). In the normal group, we found a strong positive correlation between activated memory CD4 T cells/nerve follicular helper T cells and naive B cells, neutrophils and resting mast cells and a strong negative correlation between plasma cells and naive B cells/activated memory CD4 T cells (all $p < 0.001$) (Figure 9D). Furthermore, the findings demonstrated a close relationship between F-DEGs and immune cell infiltration. In particular, CDH1 and TFAP2A were strongly negatively correlated with



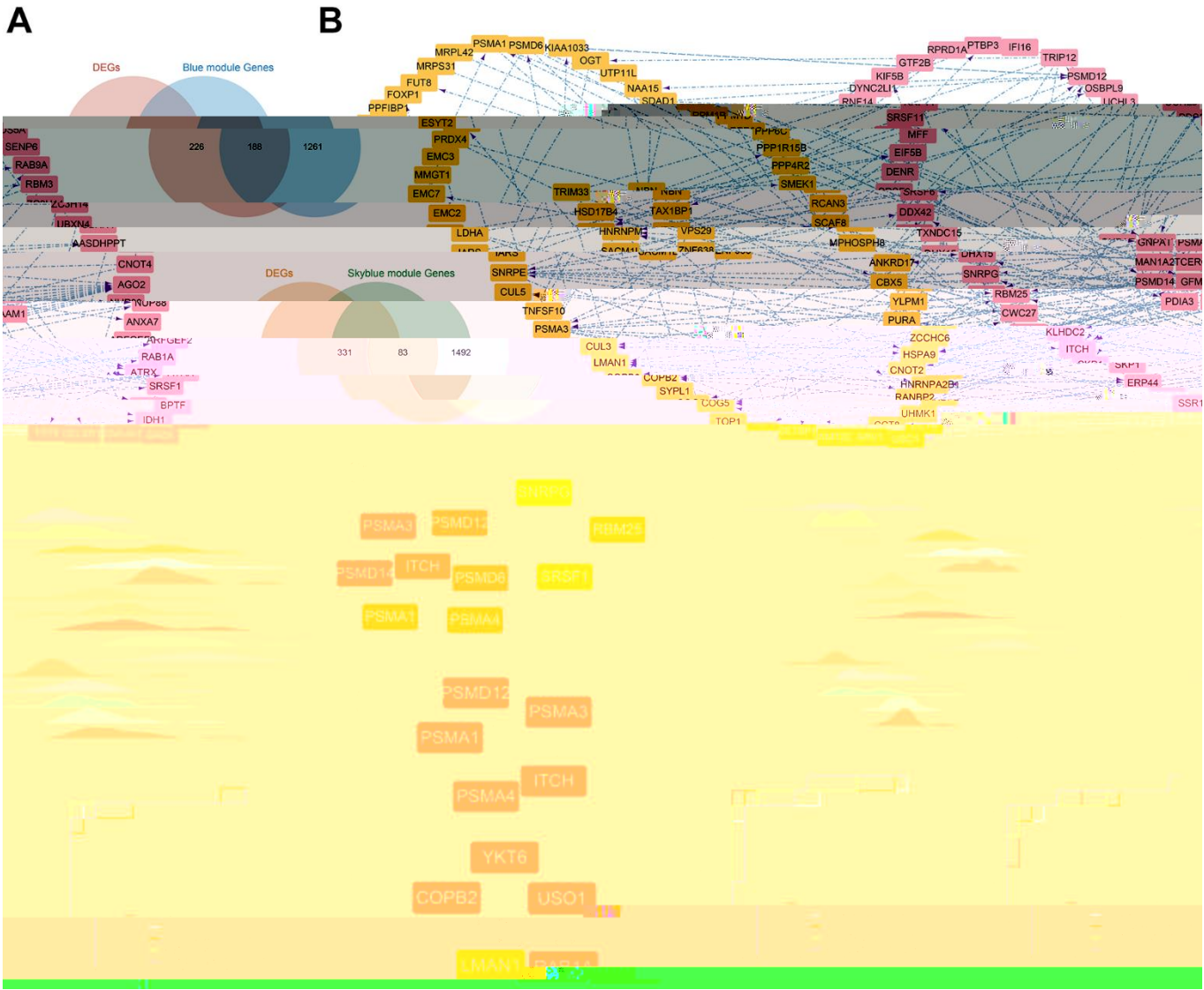
resting mast cells (all $p < 0.001$). There was also a strong positive link between resting NK cells and MDM4, as well as CD8 T cells and CDH1 (all $p < 0.01$) (Figure 9E). In the case of H-DEGs, no significantly positive correlation with immune cells was identified; however, a significantly negative connection between PSMD14 and activated dendritic cells was observed ($p < 0.01$) (Figure 9F).

Correlation analysis of DEGs in thyroid samples

By following the aforementioned data processing procedure, we obtained standardized thyroid tissue data from the GSE9340 dataset. This dataset consisted

of samples from 10 patients with TED and 8 samples from healthy controls (Figure 10A). DEGs were identified and chosen for further analysis based on the preestablished threshold (Figure 10B). Upon conducting an interaction analysis, we discovered that the genes identified in GSE9340, GSE105149, and 58331 and the ferroptosis gene set did not have any overlapping genes (Figure 10C). Overexpression of MYH11 ($p = 8.5e-3$) and APOD ($p = 0.01$) was observed in the TED group, while downregulated expression of EGR2 ($p = 0.02$) was observed in the TED group (Figure 10D).

We identified these three DEGs as T-DEGs and explored whether they were potentially related to



Z

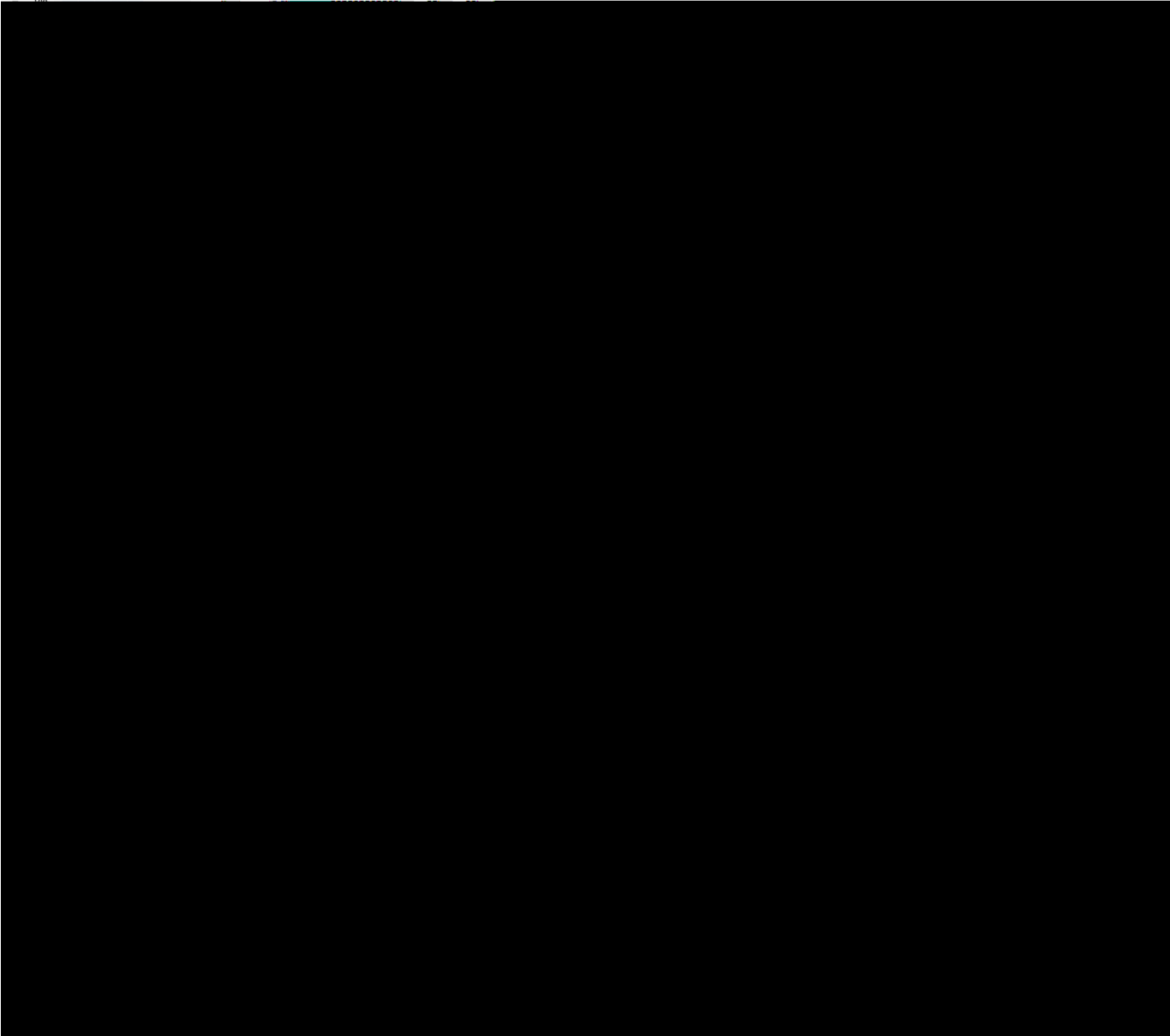
P P P

F-DEGs and H-DEGs. The results showed that EGR2 was significantly negatively correlated with IDH1 ($r = -0.68$), PEX3 ($r = -0.68$), and EMC2 ($r = -0.71$) (all $p < 0.05$) (Figure 10E). Turning to H-DEGs, we observed a significant positive correlation between MYH11 and PSMA4 ($r = 0.64$, $p < 0.05$). In addition, EGR2 was negatively correlated with all H-DEGs, especially COPB2 ($r = -0.82$, $p < 0.01$), YKT6 ($r = -0.85$, $p < 0.001$), PSMD6 ($r = -0.79$, $p < 0.01$), and PSMD14 ($r = -0.79$, $p < 0.01$) (Figure 10F).

Validation of the DEGs and immune infiltration

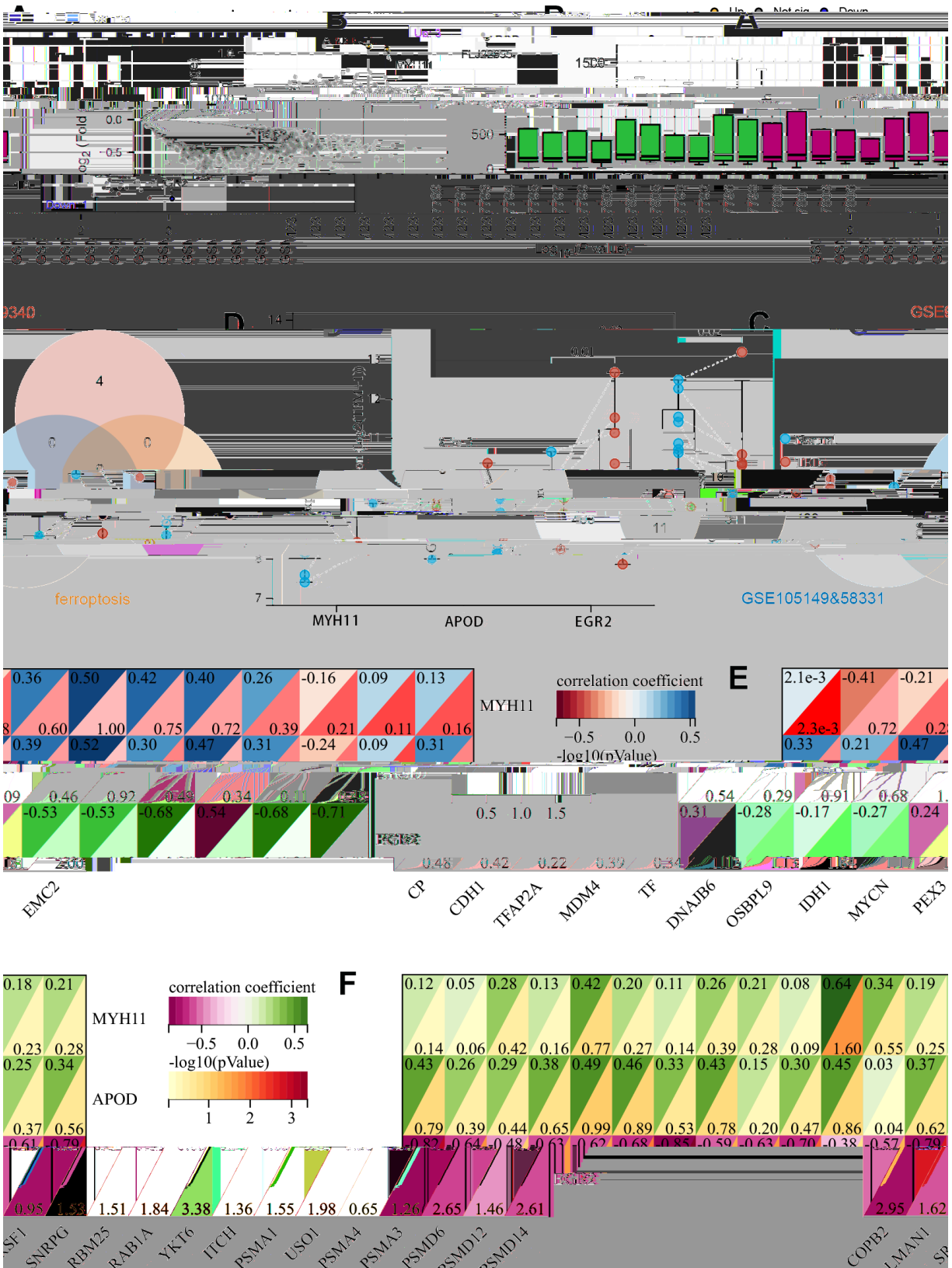
According to the computerized tomography (CT) scan, we could visually compare the degree of adipose infiltration and ocular muscle hypertrophy between the TED and normal groups. Patients with TED had obvious eye muscle hypertrophy and ocular exophthalmia (Figure 11A) compared with normal people (Figure 11B).

We further examined the expression of F-DEGs, H-DEGs, and T-DEGs in the periorbital adipose tissue.



T T S S Z Z

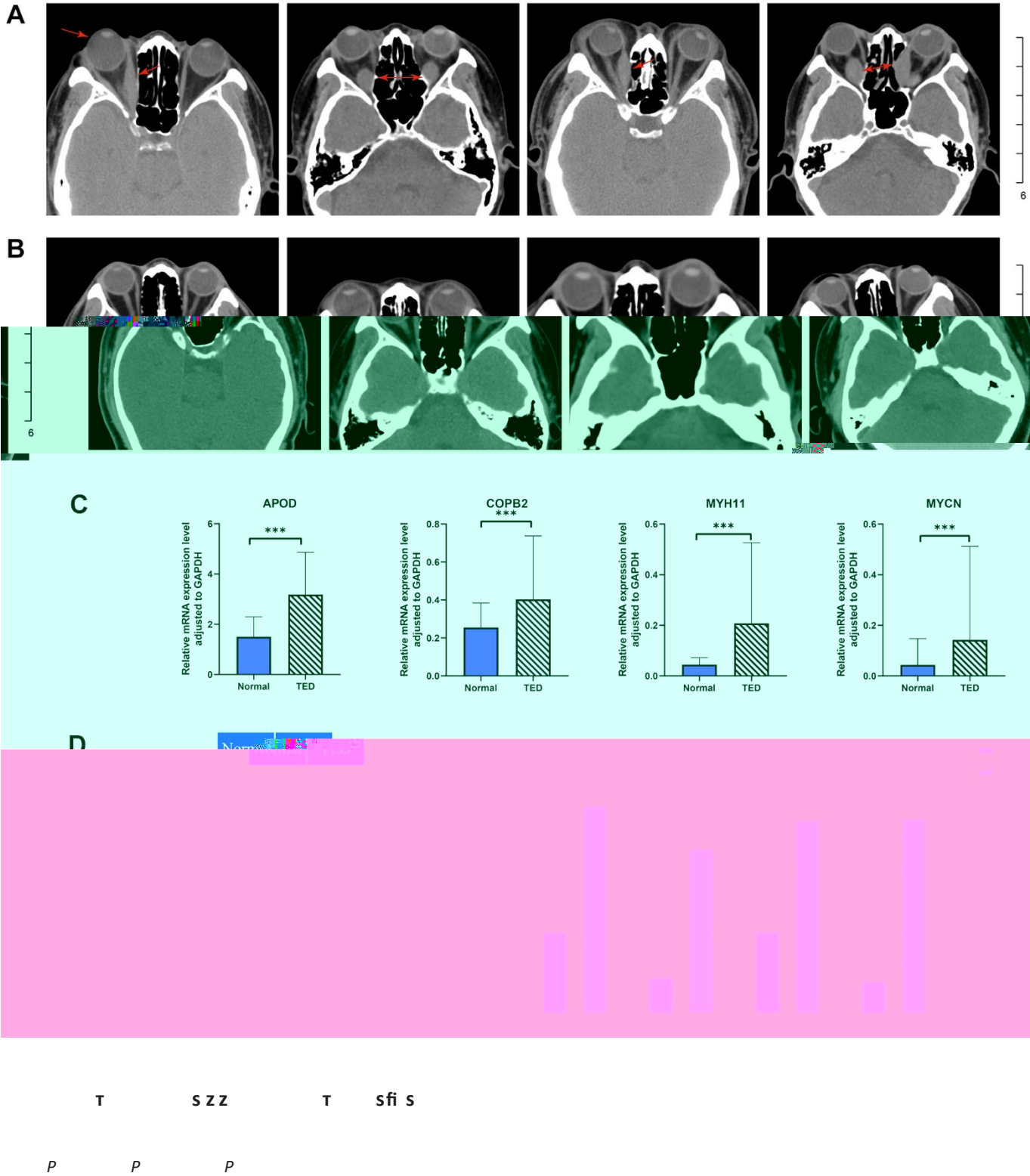
P P P



A total of 23 pairs of samples from patients with TED and normal controls were collected for qPCR validation. The expression of APOD, COPB2, MYH11, and MYCN in TED tissues was higher than that in normal tissues (all $p < 0.001$), as supported by qPCR (Figure 11C). Consistent with this result, WB further corroborated

the higher expression of these four genes in TED than in normal tissues, with a significant difference (all $p < 0.001$) (Figure 11D).

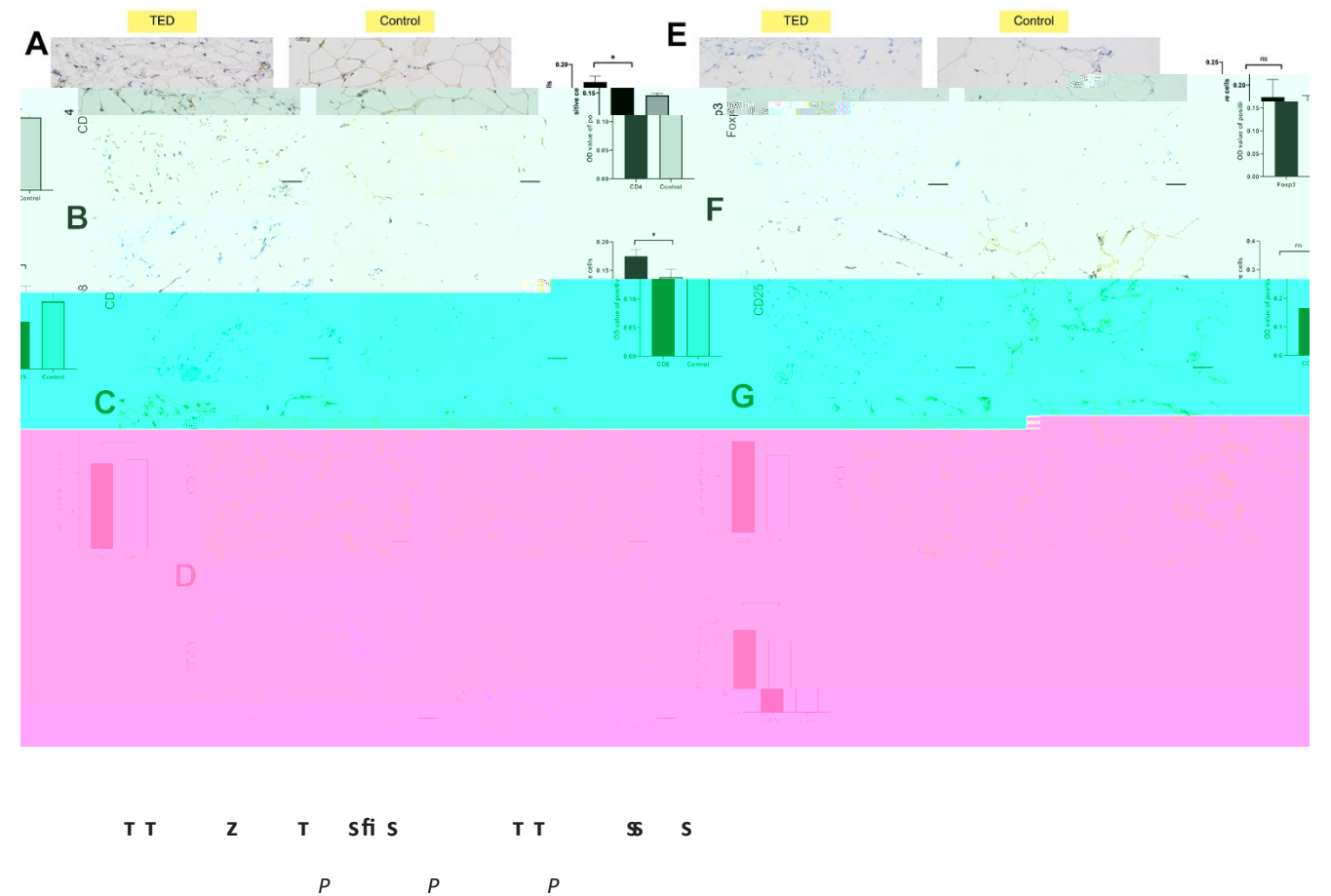
We also employed IHC to investigate the infiltration of immune cells in periorbital adipose tissue. According to



the degree of staining in the cytoplasm and nuclei, we observed obviously upregulated expression of CD4, CD8, and CD19 in TED compared with normal tissues (all $p < 0.05$) (Figure 12A 12C). However, no significant differences in the expression of CD20, Foxp3, CD25, and PC1 were observed between the TED and control groups (all $p > 0.05$) (Figure 12D 12G).

TED, as a common disease closely related to autoimmune thyroid disease, seriously affects the physical and mental health of patients [54]. In severe cases, people can even become disabled due to compression optic neuropathy or corneal decompensation [55, 56]. The pathogenesis of TED involves the deposition of hyaluronic acid and de novo synthesis of fat, resulting in orbital tissue expansion, muscle hypertrophy, and orbital inflammation caused by infiltration of various immune cells. Unfortunately, there is no cure for TED. Existing treatments, including high-dose glucocorticoid shock and orbital radiotherapy, have limited ability to alleviate the inflammatory reaction in the acute stage of the condition and are unable to rectify the long-term sequelae of the illness [57]. With the deepening of our understanding of

the molecular pathways involved in the development of TED, targeted therapy is expected to become a new method for the treatment of TED. However, except for teprotumumab [58], there has been no breakthrough in this area of research. Currently, numerous studies have provided extensive evidence indicating that ferroptosis not only serves as a crucial factor in the onset and advancement of various cancers [59–62] but also actively contributes to the development, progression, and prognosis of several major chronic diseases [63–65]. This regulated cell death process, driven by lethal lipid peroxidation, participates in various cellular metabolic processes and disease-related signaling pathways, playing an essential role in tumor suppression, immune surveillance, and ischemia-reperfusion injury, among others [66]. Despite this, the mechanism of ferroptosis in TED remains a mystery. The accompanying study may reveal a possible link between ferroptosis and the emergence of TED, along with novel diagnostic indicators or therapeutic targets to address this gap. In the current work, we discovered ferroptosis-related DEGs in TED patients and built corresponding diagnostic prediction models through deep machine learning for the first time. Subsequently, we performed enrichment analyses on F-DEGs using GO/KEGG, GSEA, and GSVA, which indicated that the relevant



molecular mechanisms were mainly focused on protein processing and transportation and hereditary material processing. Additionally, we employed WGCNA for modularization analysis of DEGs and obtained H-DEGs, which were completely different from F-DEGs. A PPI network was established, and the excellent diagnostic performance of H-DEGs was verified. Through immune infiltration analysis, special immune cells infiltrated in TED patients were identified, as were their potential correlations with the specific DEGs. Moreover, we conducted correlation analysis between T-DEGs, F-DEGs, and H-DEGs and found that EGR2 was highly negatively correlated with several DEGs in lacrimal gland samples. Adipose tissues from TED patients were also retrieved for further exploration and validation of DEG expression and immune cell infiltration.

In contrast to a previous bioinformatic study [22], our research integrated two TED-related datasets with batch effect removal to screen out brand-new DEGs. For the first time, 11 ferroptosis-related DEGs were identified as being involved in the occurrence and advancement of TED. After analyzing the expression level of every F-DEG, it was observed that all of them exhibited reduced expression in the TED group compared to the normal group, except MYCN (Figure 3A). We also revealed for the first time that these genes had an above-average diagnostic performance for TED (Figure 3B). While univariate analysis suggested that MYCN may be an effective diagnostic factor for TED (OR = 14.831, $p = 0.005$) (Figure 3C), the results of the multivariate analysis did not provide further validation. It is necessary to further validate its clinical value by expanding the sample size. Additionally, using machine learning, we constructed two pioneering ferroptosis-related diagnostic prediction models. Both of them were certified to be highly accurate and robust, with outstanding performance on clinical decisions (Figure 4). However, more clinical data should be incorporated for further validation of the reliability and precision of these models. Due to the lack of relevant data on prognosis and treatment, this study did not delve deeply into the clinical application of ferroptosis in TED therapy. However, we have planned to collaborate with more clinical centers and establish animal models to facilitate the feasibility of clinical translation practices.

According to reported studies, MYCN mutations have been strongly linked to neuroblastoma by upregulating the expression of the iron import transferrin receptor and targeting the Xc⁻ system/glutathione (GSH) pathway [67, 68]. CDH1 is associated with colorectal cancer through its involvement in the E-cadherin-NF2-Hippo-YAP signaling pathway [66, 69]. MDM4 is implicated in breast cancer by negatively regulating p53 and influencing the stress response [66, 70].

Additionally, IDH1 is involved in cholangiocarcinoma by inducing the GPX4-regulated ferroptosis pathway [66, 71, 72]. In addition to these well-established classic ferroptosis pathways, our study identified an innovative finding that F-DEGs were involved in molecular pathways of protein processing and transportation. This discovery suggests a potential interaction between the ferroptosis mechanism and protein processing in TED patients. Based on the regulated nature of the iron death mechanism, we propose that all cellular activities, including cell proliferation, metabolism, and material transportation, are subject to its regulation. However, the precise regulatory relationship, participating pathways, and core targets require further experimental validation. Our results, which are consistent with prior research, also imply an essential role of intracellular protein processing in TED progression. Our study is the first to propose the involvement of ribosome-related mechanisms and ATP synthesis coupled electron transport pathway in TED, with potential shared mechanisms with neurodegenerative diseases such as

Although some PSMD family genes were reported to be correlated with TED [22], we discovered a more comprehensive TED-related hub gene set (including six PSMD family genes) through WGCNA. Each of the H-

curves demonstrated their excellent performance for the first time (Figure 8H).

According to our knowledge, this study is the initial examination of the infiltration of immune cells in

the CIBERSORT algorithm, the TED group had a higher infiltration level of B cells, CD8 T cells, and Tregs but a lower infiltration level of plasma cells and CD4 T cells (Figure 9B). Positive correlations between M1 macrophages and naive B cells, activated mast cells and resting NK cells, and resting mast cells and M2 macrophages, as well as a negative correlation between resting memory CD4 T cells and plasma cells, were observed (Figure 9C). Potential correlations between F-DEGs and H-DEGs and immune cells were also analysed. Our analysis revealed a significant negative correlation between CDH1 and resting mast cells ($p < 0.001$), while a significant positive correlation was observed between CDH1 and CD8 T cells ($p < 0.01$). Additionally, we found a significant positive correlation between MDM4 and NK cells resting ($p < 0.01$) (Figure 9E). Although previous studies have suggested that the immune system may participate in tumor or inflammatory processes through certain key nodes of the ferroptosis pathway, the exact mechanisms remain unclear. Importantly, our study presents novel findings, as we are the first to propose the involvement

of the immune system in the pathogenesis of autoimmune disease (TED) through potential nodes of the ferroptosis pathway. Hence, it is necessary to enlarge the sample for further validation and in-depth mechanism mining.

Moreover, we innovatively assessed the potential correlations between the DEGs from two different target organs of TED patients (thyroid and lacrimal glands). EGR2, which originated from the thyroid sample, was considered to be significantly negatively correlated with several DEGs from the lacrimal gland sample. In further basic experiments, we obtained consistent expression results for four DEGs (APOD, COPB2, MYH11, and MYCN) in the periorbital adipose tissue of TED patients by qPCR and WB. According to the IHC results, we speculated that CD4 T cells, CD8 T cells, and B cells infiltrated more in the periorbital adipose tissue of TED patients than in those of normal people.

This is the first study to include the three TED effector organs for a comprehensive multidimensional interaction analysis. In our seminal work, we used more scientific data processing methods to uncover new biomarkers and potential therapeutic targets. Previous studies [18, 22, 73] only focused on DEG screening in a single type of tissue. The results of their analyses were superficial and unconvincing to some extent due to a lack of external validation. The biggest highlight of our research is that diversified analytical and validation methods were employed to connect the internal links of the three target organs and revealed four novel DEGs co-expressed in three different tissues of TED patients.

Unfortunately, the study did not include the three target organ samples from the same individual, which somewhat reduced the validity and homogeneity of the study. The main reason for this dilemma was the difficulty of human sample acquisition. We envision improving the reliability and homogeneity of our findings by constructing a TED animal model in the future. Another main weakness of this study was the paucity of the sample size. Due to the niche nature of TED, it is difficult to obtain enough clinical samples in the short term. In the future, we can further incorporate more clinical centers or build animal models to expand the sample size. Third, the study did not further explore and verify the mechanisms and pathways between target organs, novel DEGs, and immune cells due to expense limitation. The inclusion of an external validation cohort and conducting multiple functional experiments are crucial for our research. The former will enhance the robustness and generalizability of the findings, while the latter will provide a deeper understanding of the unknown molecular mechanisms. We propose

multidisciplinary collaboration and further fundamental experiments in the future to fill the gaps in this field. Despite its limitations, this study certainly adds to our understanding of TED pathogenesis. This work offers valuable insights for exploring novel targets and immune infiltration in TED.

The present study was conducted to extensively search for more valuable biomarkers and comprehensively evaluate the state of immune infiltration in TED to uncover new therapeutic approaches. The most obvious finding to emerge from this study was the discovery of previously unidentified biomarkers, namely, F-DEGs, H-DEGs, and T-DEGs, and the validation of the co-expression of APOD, COPB2, MYH11, and MYCN in three distinct target organs. Additionally, the study also revealed a strong correlation between TED pathogenesis and several types of immune cells, including CD4 T cells, B cells, and CD8 T cells. Collectively, these findings indicate that ferroptosis, along with immune injury induced by T lymphocytes and B lymphocytes, could potentially be the pivotal mechanisms implicated in TED pathogenesis. This work contributes to broadening the understanding of the molecular mechanisms underlying TED and suggests two primary areas of investigation, namely, ferroptosis and immune infiltration, as prospective focal points for further studies. The results of this research provide an experimental foundation for future investigation into the potential connection between ferroptosis, immune infiltration, and TED through a network pathway. Additionally, it illuminates the progress of novel treatment objectives for TED.

Conception and writing, Y.Y.Y.; Charting and writing, J.M.; data analysis, L.D.; reference acquisition, W.N.F.; comments and suggestions, F.H.; manuscript revision, L.D. All the authors approved the final manuscript.

The authors have declared that no conflicts of interest exist.

All procedures involving human subjects were approved by the Research Ethics Committee at Lihuili Hospital, which is associated with Ningbo University, with informed consent signed by each patient prior to enrolment (Approval No. KY2022SL408-01). This research was conducted in conformity with the Helsinki Declaration of 1964 and its subsequent amendments, as well as related ethical standards.

This study was supported by the Ningbo Health Branding Subject Fund (PPXK2018-03), the Natural Science Foundation of Ningbo (2023J221), and the Medical and Health Research Project of Zhejiang Province (2024KY1480).

Please browse Full Text version to see the data of Supplementary Table 1.

S T S Z S Z Z Z T S Z

S T S Z S Z Z Z T S Z

S T S Z S Z Z Z T S Z T S

[illegible]

S T	S	Z	T	T	Z
No.	Target	Company	Product code	Species	
	-		- -		
	-		- -		
	-		- -		
	-		- -		
			- -		
			- -		
			- -		
			- -		
	-				
	-				